Title

Fluorescing Isofunctional Ribonucleosides: Assessing Adenosine Deaminase Activity and Inhibition

Journal

ChemBioChem, 20(5)

ISSN

1439-4227

Authors

Ludford, Paul T
Rovira, Alexander R
Fin, Andrea
et al.

Publication Date

2019-03-01

DOI

10.1002/cbic.201800665

Peer reviewed

HHS Public Access

Author manuscript

Chembiochem. Author manuscript; available in PMC 2020 March 01.

Published in final edited form as:

Chembiochem. 2019 March 01; 20(5): 718–726. doi:10.1002/cbic.201800665.

Fluorescing Isofunctional Ribonucleosides: Assessing Adenosine Deaminase Activity and Inhibition

Paul T. Ludford III, **Alexander R. Rovira**, **Andrea Fin**, and **Yitzhak Tor**

Department of Chemistry and Biochemistry, University of California, San Diego, San Diego, La Jolla, California, 92093-0358, United States

Abstract

The enzymatic conversion of isothiazolo[4,3-d]pyrimidine based adenosine (^{tz}A) and 2-aminoadenosine (^{tz}2-AA) analogues to the corresponding isothiazolo[4,3-d]pyrimidine based inosine (^{tz}I) and guanosine (^{tz}G) derivatives is evaluated and compared to the conversion of native adenosine to inosine. Henri-Michaelis-Menten analyses provides the foundation for a high throughput screening assay and the efficacy of the assay is showcased via fluorescence-based analysis of ^{tz}A conversion to ^{tz}I in the presence of known and newly synthesized inhibitors.

Graphical Abstract

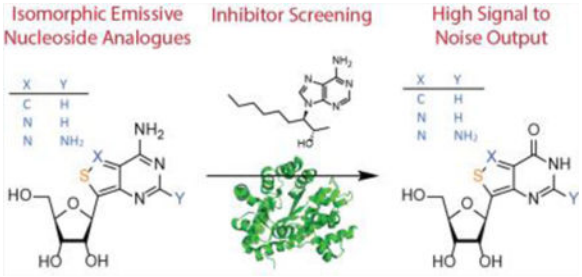

The enzymatic conversion of isothiazolo[4,3-d]pyrimidine based adenosine (^{tz}A) and 2-aminoadenosine (^{tz}2-AA) analogues to the corresponding isothiazolo[4,3-d]pyrimidine based inosine (^{tz}I) and guanosine (^{tz}G) derivatives.

Keywords

Adenosine Deaminase; Inhibitor; ^{tz}A; Adenosine; Inosine

Introduction

Recently developed isomorphic and isofunctional nucleosides with favourable fluorescent properties have proven useful in biophysical analyses and discovery assays.[1–5] The emissive features of some of these analogous nucleosides provide an effective approach to ascertain the kinetic behaviour of enzymes acting on them.[2] In particular, the search for enzyme inhibitors is facilitated as the optical interference by candidate derivatives that share a similar chromophoric skeleton as the native substrate nucleosides is minimized. The optical window that is opened up by visibly emitting substrates thus allows investigators to rely on

fast, high throughput and frequently real-time assays to assess enzymatic reactions and their inhibition.[6,7]

Adenosine deaminase (ADA), a critically important enzyme involved in purine catabolism, which deaminates adenosine to generate inosine, illustrates this concept.[8] It is a validated target for treating leukemia.[9] Pentostatin, one of its inhibitors, is currently in the clinic.[10] ADA's deamination of adenosine can be monitored by chromatographic tools (which are time consuming) or absorption spectroscopy, which suffers from optical interference by inhibitors that display absorption in the middle ultraviolet region, where adenosine itself absorbs.[11] To overcome this obstacle, a fluorescence-based inhibitor discovery assay has been demonstrated using thA, a thieno[3,4-*d*]pyrimidine based adenosine analogue (Fig. 1), where deamination and its inhibition could be continuously monitored in real time.[6]

While thA and thI, its deamination product, display distinct emission spectra, thus facilitating the fluorescence-based monitoring of the enzymatic process, thA is deaminated significantly slower than its native counterpart.[6] This shortcoming has inspired the development of a second generation of fluorescing nucleoside analogues with elevated isofunctionality, based on an isothiazolopyrimidine framework, including ^{tz}A and ^{tz}2-AA (an emissive analogue of a non-canonical nucleoside known to be an ADA substrate) (Fig. 1).[12,13]

Possessing emissive substrates with distinct enzyme affinities and deamination rates can thus allow researchers to fine tune such discovery assays to address practical aspects (i.e., adjusting the rate to match instrumental response time) or match fundamental constraints (i.e., search for inhibitors within a range of specific affinity/potency).[11,14] We thus present here the Henri-Michaelis-Menten (HMM) kinetic analyses of ADA-mediated deamination of A, ^{tz}A and ^{tz}2-AA and exploit the emissive features of the two synthetic analogues to assess the inhibitory potential on newly synthesized inhibitors based on 1-deazaadenosine.

Results and Discussion

Due to the rapidity of the ADA-mediated deamination of ^{tz}A, as shown in the pseudo-first order kinetic studies,[12] a stopped flow apparatus was used to ensure even mixing and to ultimately determine the K_m and k_{cat} values. Initial velocities of the deamination reaction were then accurately measured by fluorescence spectroscopy, relying on the different photophysical features of the substrate and product.[12] As the emission quantum yield of ^{tz}A is significantly higher than that of ^{tz}I (Fig. 1), the decrease in emission was measured over time, following excitation at 322 nm, the absorption isosbestic point of ^{tz}A and ^{tz}I. The V_{max} and K_m values were extrapolated using nonlinear regression (Fig. 2) and are listed in Table 1. The V_{max} values were plotted and fitted with a linear function followed by interpolation of the k_{cat} rate constant.

Results of the HMM analysis of ^{tz}A deamination yielded a K_m average of 18.8 ± 3.2 μM (Table 1) and V_{max} values that followed a linearly increasing trend when plotted against enzyme concentration. This fell just below the previously reported value, 29 μM, of adenosine.[6] The interpolated k_{cat} value was 263 ± 34 s^{-1}. The reported k_{cat} of adenosine is 188 s^{-1}.[15] The calculated average K_m of ^{tz}A indicated tighter enzyme binding compared to

values reported for adenosine and the interpolated k_{cat} value indicated faster conversion.[15] These results indicated the potential application of ^{tz}A for a faster high-throughput assay than previously reported for thA.[6,12]

To compare ^{tz}A to adenosine under the same conditions, the deamination of the latter to inosine was also monitored in the same stopped flow apparatus (Fig. 2). As adenosine does not fluoresce, the decrease in absorbance at 265 nm over time was measured to determine the reaction rate.[6] The V_{max} and K_m values were extrapolated using nonlinear regression (Fig. 2) and are listed in Table 1. Calculated K_m values of native adenosine were 27.8 ± 2.9, 29.5 ± 3.8, 22.8 ± 1.8, 22.8 ± 1.8, and 22.4 ± 5.5 μM for 4.1, 5.1, 6.1, 7.1, and 8.1 mU/mL enzyme concentrations resulting in an average of 25.1 ± 3.2 μM. The discrepancy in K_m values determined with the stopped flow apparatus and previously reported 29 μM may have been due to a single value being taken as opposed to the average calculated herein.[6] This was further supported by the fact that the K_m of the 4.1 mU mL^{-1} curve, the same enzyme concentration previously used, was 27.8 ± 2.9 μM, well within the experimental error of the reported 29 μM.[6]

A similar HMM kinetic analysis of the enzymatic deamination of ^{tz}2-AA to the isothiazolo[4,3-d]pyrimidine based guanosine derivative (^{tz}G) was performed using the same stopped flow apparatus. The decrease in emission was measured over time following excitation at 338 nm, the isosbestic point of ^{tz}2-AA and ^{tz}G, allowing us to determine initial velocities.[13] Unlike the other substrates, the ^{tz}2-AA HMM curve showed parabolic behaviour with increasing substrate concentration indicative of negative feedback possibly due to product inhibition (Fig. 2). As a result, a standard HMM curve did not fit the data beyond a substrate concentration of 80 μM. Potential causes could be product inhibition, photobleaching, reactive side products, etc.

In an attempt to model these observations and identify the cause, we have used the competitive inhibitor Michaelis-Menten equation. It assumes a constant inhibitor concentration with increasing substrate concentration.[17] Under product inhibition conditions, inhibitor concentration increases proportionally to substrate concentration according to a set of nonlinear differential equations.[17] To model the observed behaviour, a simplified exponential relationship between substrate and product of the form [I] = A*exp(B*[S]) was substituted for inhibitor concentration in the Michaelis-Menten competitive inhibition equation.[16] Due to the high quantum yield of ^{tz}G, an IC_{50} plot analysis of ^{tz}A to ^{tz}I conversion in the presence of increasing concentrations of ^{tz}G was performed with HPLC analysis.[12] Results showed minimal inhibition at ^{tz}G concentrations of 100 μM indicating ^{tz}G was unlikely the cause (Fig. S4).[16] The maximum possible concentration of ^{tz}G that could have formed was the starting concentration of ^{tz}2-AA. As this concentration never exceeded 126 uM, inhibition of the reaction by ^{tz}G seemed unlikely.

To showcase the potential of the fluorescence monitored ADA deamination reactions for inhibitor screening, a small number of potential inhibitors was synthesized. 1-deaza adenosine was selected as the structural core since this nucleoside and many of its derivatives are known ADA inhibitors.[18] We thus sought to make and test a number of derivatives with substitutions at the 5- and 7- carbon position, inspired by the inhibitor 5-

chloro-7-(methylamino)-9-ribosyl-imidazolopyridine (**8**).[18a] Longer alkyl chains, benzyl groups, and different substituents of the amino group had not been previously reported.

Synthesis started with 2,3-diaminopyridine (Scheme 1). Treatment with triethylorthoformate and then formic acid yielded the fused imidazolopyridine **2**,[19] which was oxidized with meta-chloroperbenzoic acid to give the *N*-oxide **3**.[19] Nitration of **3** with nitric acid at elevated temperatures produced **4**, which was treated with phosphoryl chloride to yield the dichloro derivative **5**.[19,20] Glycosylation of **5** was performed with 1,2,3,5-tetra-*O*-acetyl-β-D-ribofuranose and tin tetrachloride to produce **6**.[20] Deprotection of **6** was accomplished with methanolic ammonia to yield **7**, a common key intermediate.[20]

Various nucleophiles, including methylamine, sodium methoxide, sodium methanethiolate, propylamine, *n*-butylamine, benzylamine, and phenethylamine were added to **7** to displace the 7-chloro substituent. The chloro substituent at position 5 is far less reactive and was only successfully replaced with methoxide. The resulting derivatives were fully characterized using ^{1}H and ^{13}C NMR spectroscopy, as well as HRMS.[16] The absorption spectra of the analytically pure **8**, **9**, **10**, **11**, and **12** were measured between 220 to 600 nm.[16] To illustrate the potential spectral interference these putative inhibitors might cause, their spectra were overlaid with that of adenosine and ^{tz}A (Fig. 3), and were further expanded in Figure S3.[16] While the absorption spectrum of adenosine shows extensive overlap with that of the potential inhibitors, only minimal overlap is seen with the spectrum of ^{tz}A. This, therefore, facilitates selective excitation of the emissive adenosine analogue, ensuring a reliable fluorescence-based activity/inhibition assay.

To demonstrate the efficiency and accuracy of a screening assay utilizing ^{tz}A, inhibition studies were performed with Pentostatin and EHNA, both established inhibitors, in addition to the newly synthesized derivatives (Fig. 4, 5).[8] A preliminary screening of compounds **8**–**12** at 100 μM was performed and compounds **8** and **11**, demonstrating some potency, were further analyzed (Fig. S4, Table S1). ^{tz}A to ^{tz}I emission decline was monitored over 10 minutes. Inhibitors were added at a range of concentrations depending on the potency of the inhibitor, each in triplicate, at a substrate and ADA concentration of 3.9 μM and 4.1 mU mL^{-1}, respectively.[16] The averages of each inhibitor concentration were converted to a percentage in decimal form of uninhibited ^{tz}A to ^{tz}I conversion and then plotted on a semi-log axes (Fig. 4, 5).

Generated inhibitor IC_{50} plots were fitted with a sigmoidal Hill curve yielding IC_{50} values of 1.44 ± 0.14 nM, 23.2 ± 4.2 nM, 21 ± 8 μM, and 220 ± 70 μM for Pentostatin, EHNA, **8**, and **11** respectively (Fig. 4,5). Transformation of the IC_{50} values to K_I values with the Cheng-Prusoff equation gave 1.19 ± 0.15 nM, 19.2 ± 4.0 nM, 18 ± 7 μM, and 190 ± 70 μM for Pentostatin, EHNA, **8**, and **11**, respectively.[21] The determined IC_{50} and K_I values of Pentostatin, EHNA, and **8** were in good agreement with previously reported values demonstrating the accuracy of the assay.[6,8,18a] The IC_{50} of **8**, a previously synthesized and analyzed inhibitor, was higher than the reported value.[18a] The absorption spectra of **8** was shown to overlap with the spectra of adenosine (Fig. 3).[18a] Since previous analyses of **8** were performed using absorption measurements, spectral interference could potentially account for such discrepancies.[18a] As ^{tz}A primarily absorbs and fluoresces at longer

wavelengths than the inhibitors, a higher degree of accuracy was possible.[18a,c] While a rather impotent inhibitor, **11** was newly synthesized and tested with this assay. As with **8**, the absorption spectrum of **11** significantly overlaps with that of adenosine. In contrast, the absorption spectrum of ^{tz}A did not overlap with the spectrum of the inhibitor in the range used by the screening assay providing a more robust screening.

Conclusions

Michaelis-Menten analyses of the ADA-mediated deamination reactions of adenosine, ^{tz}A, and ^{tz}2-AA were conducted. V_{max} and K_m values were determined for adenosine and ^{tz}A and a product inhibition curve was fit to ^{tz}2-AA V_0 data. A k_{cat} value was interpolated for ^{tz}A. Several potential inhibitors of ADA based on 1-deazaadenosine were synthesized. An IC_{50} analyses of Pentostatin, EHNA, **8**, and **11** were performed and IC_{50} values of Pentostain, EHNA, and **8** were in good standing with previously reported values. One of the newly synthesized derivatives, **11**, was determined to be a weak inhibitor of ADA.

Overall, two new ADA inhibitor discovery assays were established. Similar to the previously established assay, the two adenosine analogues absorb primarily above 300 nm, outside of the optical absorption range of most ADA inhibitors. Additionally, each adenosine analogue has its own conversion rate as well as unique absorption and emission spectra thus allowing one to adjust signal intensity, wavelength range, and reaction time. This was showcased by the use of one assay to analyse two well established inhibitors, EHNA and Pentostatin, and compare with an already established assay.[6] Likewise, another known inhibitor, **8**, was re-evaluated using the new assay and compared with a previously reported value determined with adenosine.[18a] Finally, a new inhibitor, **11**, was discovered using the newly established assay.

Experimental Section

Materials and Methods:

Reagents were purchased from Sigma-Aldrich, TCI, and Acros and were used without further purification unless otherwise specified. Solvents were purchased from Sigma-Aldrich and Fisher Scientific, and dried by standard techniques. NMR solvents were purchased from Cambridge Isotope Laboratories (Andover, MA). All reactions were monitored with analytical TLC (Merck Kieselgel 60 F_{254}). Column chromatography was carried out with Teledyne ISCO Combiflash Rf with silica gel particle size 40–63 um. NMR spectra were obtained on Varian Mercury 300 MHz and Varian VX 500 MHz. Mass spectra were obtained on an Agilent 6230 HR-ESI-TOF MS at the Mass Spectrometry Facility at the UCSD Chemistry and Biochemistry Department.

Key Intermediate 7:

Compounds **2**–**7** were synthesized based on previously published procedures[19,20] and **1** was purchased from Sigma-Aldrich.

5-chloro-7-methylamino-1-deaza-purine riboside (8):

Solid **7** (10 mg, 0.031 mmol) was placed in a pressure vial (8 mL) and then dissolved in methylamine in ethanol (33wt%, 2 mL, 16 mmol, 520 eq.) while stirring. The vial was capped and the mixture brought to 80^{O}C and stirred for 48 hours. The mixture was allowed to cool and the solvent evaporated off. The resulting residue was purified using column chromatography with a gradient of 0 to 10% MeOH in DCM (R_f: 0.3 in 10% MeOH in DCM) yielding **8** as a glassy, clear solid (8.2 mg, 84%). ^{1}H NMR (300 MHz, CD_3OD): δ 8.22 (s, 1H), 6.43 (s, 1H), 5.94 (d, *J* = 6.4 Hz, 1H), 4.78 (t, *J* = 6.0 Hz, 1H), 4.34 (dd, *J* = 5.0, 2.6 Hz, 1H), 4.18 (q, *J* = 2.4 Hz, 1H), 3.91, 3.77 (ABq, *J* = 12.6 Hz, 2H), 3.01 (s, 3H). ^{13}C NMR (125 MHz, CD_3OD): δ 149.10, 147.15, 144.10, 139.96, 139.88, 122.75, 97.50, 89.92, 86.57, 73.52, 71.23, 62.19. ESI-HRMS calculated for $C_{12}H_{15}ClN_4O_4$ $[M+H]^+$ 315.0855, found 315.0854.[16,18a]

5-chloro-7-methylthio-1-deaza-purine riboside (9):

Solid **7** (7.6 mg, 0.024 mmol) was placed in a pressure vial and flushed with argon. Sodium methanethiolate in MeOH (0.5 M, 2 mL, 1.0 mmol, 42 eq.) was added to the mixture and then stirred at 105^{O}C for 24 hours. The mixture was cooled and the solvent evaporated off. The resulting residue was purified with column chromatography with a gradient of 0 to 10% MeOH in DCM (R_f: 0.5 in 10% MeOH in DCM) yielding **9** as a pale yellow solid (6.7 mg, 84%). ^{1}H NMR (300MHz, CD_3OD): δ 8.57 (s, 1H), 7.19 (s, 1H), 6.07 (d, *J* = 5.7 Hz, 1H), 4.73 (t, *J* = 5.4 Hz, 1H), 4.37 (t, *J* = 4.5 Hz, 1H), 4.18 (q, *J* = 3.1 Hz, 1H), 3.92, 3.80 (ABq, *J* = 12.3 Hz, 2H), 2.67 (s, 3H). ^{13}C NMR (125MHz, CD_3OD): δ 146.20, 146.02, 143.17, 142.75, 131.52, 112.37, 89.43, 86.07, 73.99, 70.75, 61.69, 11.98. ESI-HRMS calculated for $C_{12}H_{14}ClN_3O_4S$ $[M–H]^-$ 330.0321, found 330.0320.[16]

5,7-dimethoxy-1-deaza-purine riboside (10):

Solid **7** (7.8 mg, 0.025 mmol) was placed in a pressure vial and flushed with argon. Sodium methoxide in MeOH (2 mL, 0.5M, 40 eq.) was added to the mixture and then stirred at 105^{O}C for 24 hours. The mixture was cooled and then placed under vacuum to remove excess solvent. The resulting residue was purified with column chromatography with a gradient of 0 to 10% MeOH in DCM (R_f: 0.4 in 10% MeOH in DCM) yielding **10** as a pale yellow solid (2.0 mg, 26%). ^{1}H NMR (300MHz, CD_3OD): δ 8.26 (s, 1H), 6.30 (s, 1H), 6.06 (d, *J* = 5.3 Hz, 1H), 4.81 (t, *J* = 5.3 Hz, 1H), 4.42 (t, *J* = 4.5 Hz, 1H), 4.11 (dd, *J* = 7.9, 3.9 Hz, 1H), 4.03 (s, 3H), 3.98 (s, 3H), 3.88, 3.78 (ABq, *J* = 12.0 Hz, 2H). ^{13}C NMR (125MHz, CD_3OD): δ 163.71, 159.66, 144.59, 139.05, 120.86, 88.67, 88.02, 85.14, 73.75, 70.57, 61.62, 55.15, 53.15. ESI-HRMS calculated for $C_{13}H_{17}N_3O_6$ $[M+Na]^+$ 334.1010, found 334.1007.[16]

5-chloro-7-benzylamino-1-deaza-purine riboside (11):

Solid **7** (7.9 mg, 0.025 mmol) was placed in a pressure vial and flushed with argon. *n*-Butanol (2 mL) and benzylamine (0.11 mL, 1.0 mmol, 40 eq.) were added to the mixture and then stirred at 90^{O}C for 24 hours. The mixture was cooled and the excess solvent removed under vacuum. The resulting residue was purified with column chromatography with a gradient of 0 to 5% MeOH in DCM (R_f: 0.3 in 5% MeOH in DCM) yielding **11** as a

glassy yellow solid (8.5 mg, 87%). ^{1}H NMR (300MHz, CD_3OD): δ 8.25 (s, 1H), 7.45–7.25 (m, 5H), 6.42 (s, 1H), 5.94 (d, *J* = 6.4 Hz, 1H), 4.77 (t, *J* = 6.0 Hz, 1H), 4.62 (s, 2H), 4.33 (dd, *J* = 5.1, 2.6 Hz, 1H), 4.18 (q, *J* = 2.6 Hz, 1H), 3.92, 3.76 (ABq, *J* = 12.5 Hz, 2H). ^{13}C NMR (125MHz, CD_3OD): δ 149.10, 147.15, 144.10, 139.96, 122.75, 97.50, 89.92, 86.57, 73.52, 71.23, 62.19, 20.65. ESI-HRMS calculated for $C_{18}H_{19}ClN_4O_4$ $[M–H]^-$ 389.1022, found 389.1019.[16]

5-chloro-7-butylamino-1-deaza-purine riboside (12):

Solid **7** (8.2 mg, 0.026 mmol) was placed in a pressure vial and flushed with argon. *n*-Butanol (2 mL) and n-butylamine (0.1 mL, 1.0 mmol, 38 eq.) were added to the mixture and then stirred at 90^{o}C overnight. The mixture was cooled and the solvent evaporated off with a rotary evaporator. The resulting residue was purified with column chromatography with a gradient of 0 to 10% MeOH in DCM (R_f: 0.4 in 10% MeOH in DCM) yielding **12** as a glassy solid (4.1 mg, 44%). ^{1}H NMR (300MHz, CD_3OD): δ 8.23 (s, 1H), 6.45 (s, 1H), 5.93 (d, *J* = 6.4 Hz, 1H), 4.77 (t, *J* = 6.0 Hz, 1H), 4.34 (dd, *J* = 5.0, 2.6 Hz, 1H), 4.18 (q, *J* = 2.5 Hz, 1H), 3.92, 3.76 (ABq, *J* = 12.5 Hz, 2H), 3.38 (t, *J* = 6.9 Hz, 2H), 1.79 – 1.63 (m, 2H), 1.51 (dq, *J* = 14.3, 7.2 Hz 2H), 1.02 (t, *J* = 7.3 Hz, 3H). ^{13}C NMR (125MHz, CD_3OD): δ 149.10, 147.15, 144.10, 139.96, 122.75, 97.50, 89.92, 86.57, 73.52, 71.23, 62.19, 20.65. ESI-HRMS calculated for $C_{15}H_{21}ClN_4O_4$ $[M+H]^+$ 357.1324, found 357.1320.[16]

Henri-Michaelis-Menten Kinetics General Methods:

Bovine spleen ADA was obtained from Sigma Aldrich (EC Number 232–817-5). The commercial solution [1150 U mL^{-1} in 3.2 M $(NH_4)_2SO_4$, 0.01 M potassium phosphate, pH 6.0] was diluted to 1.15 U mL^{-1} by dissolving an aliquot (1 μL) in phosphate buffer (999 μL, 50 mM, pH 7.4). The enzyme stock solution was freshly prepared and kept on ice prior to use. The enzyme stock solution was diluted to concentrations of 4.5, 5.6, 6.7, 7.8, and 8.9 mU mL^{-1} with phosphate buffer. A total of 20 μL enzyme solution was mixed with 200 μL of substrate solution in the stopped flow apparatus chamber yielding final enzyme concentrations of 4.1, 5.1, 6.1, 7.1, and 8.1 mU mL^{-1}.

Concentrated stock solutions (3.7 mM, 4.1 mM) in DMSO were prepared for ^{tz}A and ^{tz}2-AA. A 1.0 mM solution was prepared for ^{tz}A and ^{tz}2-AA from the concentrated stock solutions and autoclaved water. A 1.0 mM solution of adenosine was prepared in autoclaved water from solid adenosine.

The ADA-mediated enzymatic conversion of adenosine (and its analogs) was followed by absorbance and emission (for the emissive analogs ^{tz}A and ^{tz}2-AA) spectroscopy by monitoring the intensity variation for absorbance and voltage output for emission as a function of time. The real-time conversion of adenosine (and its analogs) to inosine (and its analogs) were performed on an Applied Photophysics Pistar Stop Flow Apparatus.

Stopped Flow Fluorescence Measurements and HMM Kinetic Analysis of Enzymatic Conversion of ^{tz}A to ^{tz}I:

Substrate concentrations ranging from 3.9 to 34.5 μM were used keeping the enzyme concentration constant at 4.1 – 8.1 mU mL^{-1}. Upon excitation at 322 nm with a bandwidth

of 2 nm substrate concentration voltage output (V) decrease was measured over 50 seconds. The photo multiplication unit (PMU) was set to 550.

Data points were fit with a linear approximation in MatLab to determine the rate of conversion V_0 (V s^{-1}) and the initial voltage output. An average of the initial voltage output for each substrate concentration was plotted against the substrate concentration producing a linear slope. The linear slope was used to convert all voltage output vs. time plots to concentration vs. time plots. Linear approximation of the concentration vs. time plots yielded the rate of conversion V_0 ([S] s^{-1}). The average value for the rate of conversion V_0 ([S] s^{-1}) for each substrate concentration measured in triplicate was plotted as a function of substrate concentration. V_{max} was extrapolated from the rate of conversion vs. substrate concentration plots using KaleidaGraph and Michaelis-Menten fitted non-linear regression. The K_M of each plot was determined by taking the substrate concentration at half V_{max}. The V_{max} of each enzyme concentration was plotted to yield a V_{max} vs. enzyme concentration plot. The plot was fit with a linear approximation providing the slope (k_{cat}).

Stopped Flow Absorbance Measurements and HMM Kinetic Analysis of Enzymatic Conversion of A to I:

Substrate concentrations ranging from 3.9 to 34.5 μM were used keeping the enzyme concentration constant at 4.1 – 8.1 mU mL^{-1}. Absorbance was measured over 50 seconds at a wavelength of 265 nm. Data points were fit with a linear approximation in MatLab to determine the rate of conversion V_0 (mAbs s^{-1}). The average values for the rate of conversion V_0 (Abs s^{-1}) for each substrate concentration measured in triplicate were plotted as a function of substrate concentration. V_{max} was extrapolated from the rate of conversion (mAbs s^{-1}) vs. concentration plots using KaleidaGraph and Michaelis-Menten fitted non-linear regression. The K_M of each plot was determined by taking the substrate concentration at half V_{max}.

Stopped Flow Fluorescence Measurements and HMM Kinetic Analysis of Enzymatic Conversion of ^{tz}2-AA to ^{tz}G:

Substrate concentrations ranging from 3.9 to 126 μM were used keeping the enzyme concentration constant at 4.1 mU mL^{-1}. Upon excitation at 338 nm with a bandwidth of 2 nm substrate concentration voltage output (V) decrease was measured over 50 seconds. The photo multiplication unit (PMU) was set to 450. Data points were fit with a linear approximation in MatLab to determine the rate of conversion V_0 (V s^{-1}). The average values for the rate of conversion V_0 (V s^{-1}) for each substrate concentration measured in triplicate were plotted as a function of substrate concentration. In order to model product inhibition, a makeshift function[16] (see SI) was fit to the data using nonlinear regression to approximate the K_M, K_I, and V_{max} of the resulting curve. The function was developed from the Michaelis-Menten competitive inhibition equation substituting an exponential relationship[16] (see SI) between product and substrate for [I].

Screening of Potential Inhibitors:

The ADA-mediated enzymatic conversion of ^{tz}A in the presence of inhibitor was followed by emission spectroscopy by monitoring the emission intensity signal at 410 nm upon

excitation at 322 nm (the isosbestic point determined by absorption spectroscopy). The real-time conversion of ^{tz}A to ^{tz}I was measured on a Horiba Fluoromax-4 equipped with a cuvette holder with a built-in stirring system, setting the excitation and emission slits at 3 nm respectively and taking a point every two seconds for 600 seconds upon addition of ADA.

Each potential inhibitor was screened with ^{tz}A conversion to ^{tz}I in the presence of ADA. Concentrated stock solutions of each potential inhibitor were prepared in water and DMSO. An aliquot of the ^{tz}A 1.0 mM stock solution and an aliquot of a potential inhibitor stock solution was added to phosphate buffer (50mM, 7.4 pH) in a 3 mL cuvette for a final ^{tz}A concentration of 3.9 μM and a final potential inhibitor concentration of 100 μM. Upon excitation at 322 nm and observation of emission at 410 nm an aliquot of ADA stock solution was added and emission observed for 600 seconds. Each resulting emission vs. time plot was normalized relative to the blank (no inhibitor present) setting the initial intensity to 0 and the maximum intensity change as 1.[16]

Potential Inhibitor Absorption Spectra:

Spectroscopic grade DMSO was obtained from Sigma Aldrich and aqueous solutions were prepared with de-ionized water. All the measurements were carried out in a 1 cm four-sided quartz cuvette from Helma.

Absorption spectra were measured on a Shimadzu UV-2450 spectrophotometer setting the slit at 1 nm and using a resolution of 0.5 nm. All the spectra were corrected for the blank. The instrument was equipped with a thermostat controlled ethylene glycol-water bath fitted to specially designed cuvette holder and the temperature was kept at 25.0 ± 0.1^{O}C.

Inhibitors were dissolved in water and a small portion of DMSO if necessary to prepare highly concentrated stock solutions: **8** (1.6 mM), **9** (6.0 mM), **10** (4.2 mM), **11** (2.3 mM), **12** (1.0 mM). In a typical experiment, aliquots of the respective concentration stock solutions were diluted with air-saturated water to yield a final concentration of 0.1 M and a total volume of 125 μL. The solutions were mixed with a pipette for 10 seconds and placed in the cuvette holder at 25.0 ± 0.1^{O}C for 3 minutes before spectra were recorded. The percent by volume of DMSO for each sample were: **9** (0.05 v/v%), **11** (0.1 v/v%), **12** (0.03 v/v%).[16]

HPLC Analysis of ADA Activity In the Presence of ^{tz}G:

In order to confirm ^{tz}G inhibition of ADA, inhibition studies were performed on ^{tz}G. As ^{tz}G is fluorescent and has a higher quantum yield than ^{tz}A and ^{tz}I, inhibition had to be tested using HPLC. ^{tz}A was converted to ^{tz}I in the presence of ADA in the presence of increasing concentrations of ^{tz}G. For each experiment, the commercial solution (1150 U/mL in 3.2 M $(NH_4)_2SO_4$, 0.01 M potassium phosphate, pH 6.0) was diluted to 1.15 U/mL by dissolving an aliquot (1 μL) in phosphate buffer (999 μL, 50 mM, pH 7.4). The enzyme stock solution was freshly prepared and kept on ice prior to use. Stock solutions of 1 mM ^{tz}A and 1 mM ^{tz}G were prepared. An aliquot of ^{tz}G and the appropriate amount of phosphate buffer were mixed to arrive at concentrations of 0, 0.1, 1, 10, and 100 μM and then an aliquot of ^{tz}A (5.9 μL) was added for a final concentration of 3.9 μM. An aliquot of ADA (5.4 μL) was added for a total of 1500 μL and concentration of 4.1 mU mL^{-1}. After allowing the reaction to

proceed for 10 minutes the mixture was frozen in a –78°C bath. The reaction was then reheated to liquid and immediately placed in the HPLC for separation and analysis.

HPLC analysis was performed with an Agilent 1200 series system with a Sepax Bio-C18 5μm, 4.6 × 250 mm column. Stock solutions of 0.1% TFA were prepared by dissolving 1 mL of TFA (99%) in 999 mL MilliQ water or HPLC grade acetonitrile and filtered using Millipore type GNWP 0.2 μm filters before use. Injections of 15 μL were subjected to a gradient of 0.5% to 5% acetonitrile 0.1% TFA in water 0.1% TFA over 25 minutes. The column was then flushed for 10 minutes. Each experiment was run at 1 mL/min at 25°C. Each run was monitored at 260, 315, and 333 nm with calibrated references at 650 nm and a slit width of 1 nm.

The area under each ^{tz}A peak was integrated and plotted as percent inhibition normalized to the blank. Each curve was compared to a standard run performed with ^{tz}A alone. Results showed little change in area of the ^{tz}A peak. This suggested ^{tz}G was not a potent enough inhibitor to cause the drop in initial rate of the ^{tz}2-AA ADA reaction at higher concentrations.[16]

Supplementary Material

Refer to Web version on PubMed Central for supplementary material.

Acknowledgements

We thank the National Institutes of Health for generous support (via grant number GM 069773), the Chemistry & Biochemistry MS Facility, and the UCSD NMR Facility.

Abbreviations:

DCM	dichloromethane
DMF ***N***	***N***-dimethylformamide
MeOH	methanol
TFA	Trifluoroacetic acid
DMSO	Dimethyl sulfoxide
ACN	Acetonitrile
TAR	Tetra-*O*-acetyl-β-D-ribofuranose

References

[1]. (a)Wilson JN and Kool ET, Org. Biomol. Chem, 2006, 4, 4265–4274 [PubMed: 17102869] (b)Hawkins ME, Cell Biochem. Biophys, 2001, 34, 257–281 [PubMed: 11898867] (c)Wilhelmsson LM, Q. Rev. Biophys, 2010, 43, 159–183 [PubMed: 20478079] (d)Wierzchowski J, Antosiewicz JM and Shugar D, Mol. BioSyst, 2014, 10, 2756–2774 [PubMed: 25124808] (e)Kimoto M, Cox RS and Hirao I, Expert Rev. Mol. Diagn, 2011, 11, 321–31 [PubMed: 21463241] (f)Okamoto A, Saito Y and Saito I, J. Photochem. Photobiol. C Photochem. Rev, 2005, 6, 108–122(g)Xu W, Chan K and Kool E, Nat. Chem, 2017, 9, 1043–

1055 [PubMed: 29064490] (h)Saito Y and Hudson R, J. Photochem. Photobiol. C Photochem. Rev, 2018, 36, 48–73.

[2]. Jones AC and Neely RK, Q. Rev. Biophys, 2015, 48, 244–279. [PubMed: 25881643]

[3]. Sinkeldam RW, Greco N and Tor Y, Chem. Rev, 2010, 110, 2579–2619. [PubMed: 20205430]

[4]. (a)Seio K, Kanamori T and Masaki Y, Tetrahedron Lett, 2018, 59, 1977–1985(b)Maiti M, Michielssens S, Dyubankova N, Maiti M, Lescrinier E, Ceulemans A, and Herdewijn P, Chem. A Eur. J, 2012, 18, 857–868.

[5]. Rovira AR, Fin A and Tor Y, J. Am. Chem. Soc, 2017, 139, 15556–15559 [PubMed: 29043790] (j)Hallé F, Fin A, Rovira AR and Tor Y, Angew. Chem. Int. Ed, 2018, 57, 1087–1090.

[6]. Sinkeldam RW, McCoy LS, Shin D and Tor Y, Angew. Chem. Int. Ed, 2013, 52, 14026–14030.

[7]. a)Lin S, Gao W, Tian Z, Yang C, Lu L, Mergny J, Leung C, and Ma D, Chem. Sci, 2015, 6, 4284–4290 [PubMed: 29218197] b)Hori Y, Otomura N, Nishida A, Nishiura M, Umeno M, Suetake I, and Kikuchi K, J. Am. Chem. Soc, 2018, 140, 1686–1690 [PubMed: 29381073] c)Collot M, Fam TK, Ashokkumar P, Faklaris O, Galli T, Danglot L, and Klymchenko AS, J. Am. Chem. Soc, 2018, 140, 5401–5411 [PubMed: 29446627] d)Vellaisamy K, Li G, Ko C, Zhong H, Fatima S, Kwan H, Wong C, Kwong W, Tan W, Leung C, Ma D, Chem. Sci, 2018, 9, 1119–1125 [PubMed: 29675156] e)Wang W, Wu C, Yang C, Li G, Han Q, Li S, Lee SM, Leung C, Ma D, Sens. Actuator B-Chem, 2018, 255, 1953–1959f)Wang M, Mao Z, Kang T, Wong C, Mergny J, Leung C, Ma D, Chem. Sci, 2016, 7, 2516–2523. [PubMed: 28660021]

[8]. Cristalli G, Costanzi S, Lambertucci C, Lupidi G, Vittori S, Volpini R and Camaioni E, Med. Res. Rev, 2001, 21, 105–128. [PubMed: 11223861]

[9]. Glazer RI, Cancer Chemother. Pharmacol, 1980, 4, 227–235. [PubMed: 7002342]

[10]. O'Dwyer PJ, Wagner B, Leyland-Jones B, Wittes RE, Cheson BD and Hoth DF, Ann. Intern. Med, 1988, 108, 733–743. [PubMed: 3282467]

[11]. (a)Sprecher CA and Johnson WC, Biopolymers, 1977, 16, 2243–2264 [PubMed: 334279] (b)Callis PR, Ann. Rev. Phys. Chem, 1983, 34, 329–357(c)Peon J and Zewail AH, Chem. Phys. Lett, 2001, 348, 255–262(d)Onidas D, Markovitsi D, Marguet S, Sharonov A and Gustavsson T, J. Phys. Chem. B, 2002, 106, 11367–11374(e)Cohen B, Crespo-Hernández CE, Kohler B, Crespo-Hernandez CE and Kohler B, Faraday Discuss, 2004, 127, 137–147. [PubMed: 15471343]

[12]. Rovira AR, Fin A and Tor Y, J. Am. Chem. Soc, 2015, 137, 14602–14605. [PubMed: 26523462]

[13]. Rovira AR, Fin A and Tor Y, Chem. Sci, 2017, 8, 2983–2993. [PubMed: 28451365]

[14]. (a)Lakowicz JR, Principles of fluorescence spectroscopy, 3rd Edition, Springer, New York, 2006, 63–97(b)Valeur B, Molecular Fluorescence, Principles and Applications, Wiley-VCH, Weinheim, 2002, 273–378.

[15]. Ford H, Dai F, Mu L, Siddiqui MA, Nicklaus MC, Anderson L, Marquez VE and Barchi JJ, Biochemistry, 2000, 39, 2581–2592. [PubMed: 10704207]

[16]. See supporting information.

[17]. Johnson KA and Goody RS, Biochemistry, 2011, 50, 8264–8269. [PubMed: 21888353]

[18]. (a)Cristalli G, Eleuteri A, Vittori S, Volpini R, Camaioni E and Lupidi G, Drug Dev. Res, 1993, 28, 253–258(b)Cristalli G, Vittori S, Eleuteri A, Volpini R, Camaioni E, Lupidi G, Mahmood N, Bevilacqua F and Palù G, J. Med. Chem, 1995, 38, 4019–4025 [PubMed: 7562937] (c)Antonini I, Cristalli G, Franchetti P, Grifantini M, Martelli S, Lupidi G and Riva F, J. Med. Chem, 1984, 27, 274–278 [PubMed: 6699873]

[19]. Maiti M, Michielssens S, Dyubankova N, Maiti M, Lescrinier E, A. C. and P. H., Chem. A Eur. J, 2012, 18, 857–868.

[20]. Cristalli G, Grifantini M, Vittori S, Balduini W and Cattabeni F, Nucleotides and Nucleosides, 1985, 4, 625–639.

[21]. Yung-Chi C and Prusoff WH, Biochem. Pharmacol, 1973, 22, 3099–3108. [PubMed: 4202581]

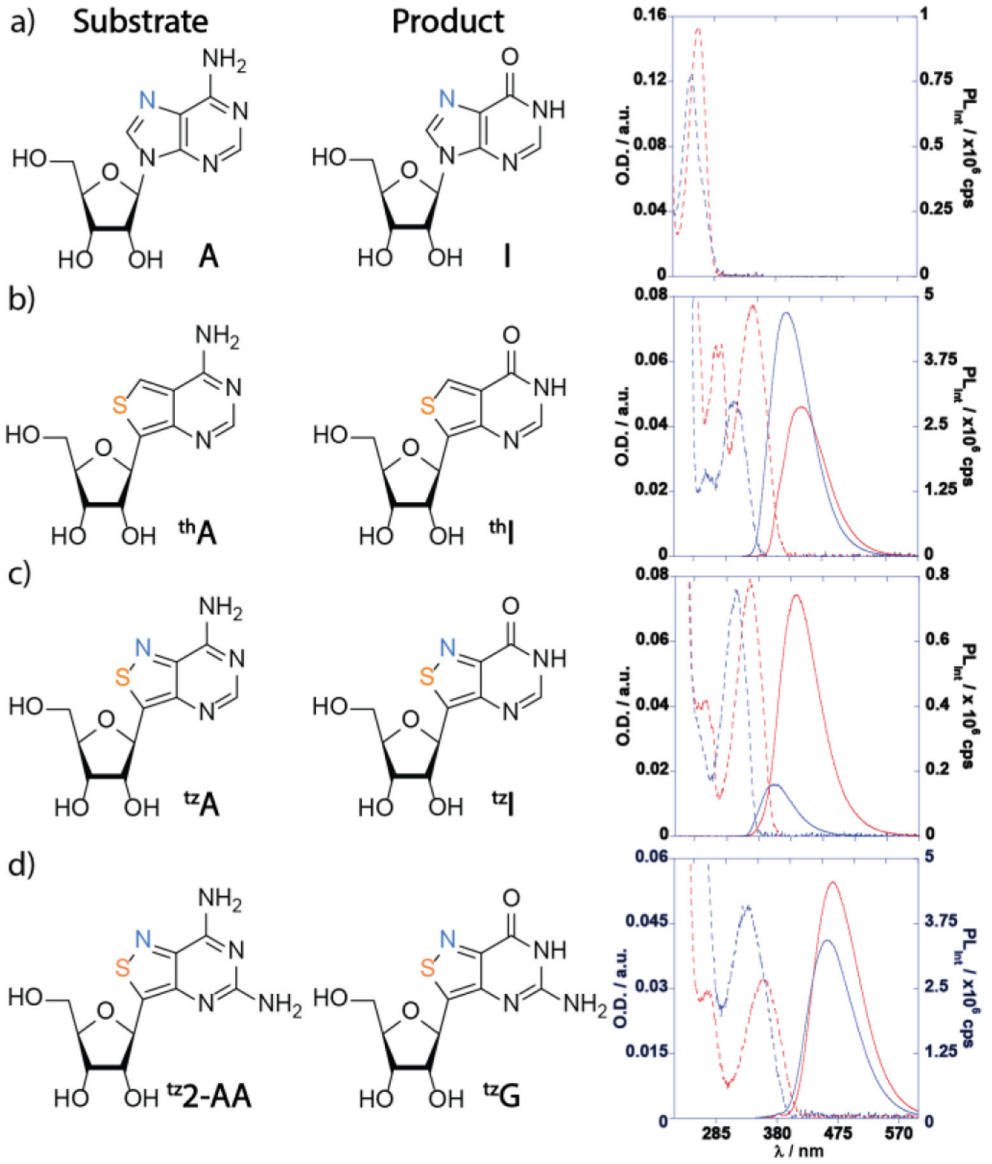

Figure 1.

Structure, absorption (dashed), and emission (solid) spectra of a) A (red) and I (blue) b) thA (red) and thI (blue) c) ^{tz}A (red) and ^{tz}I (blue) d) ^{tz}2-AA (red) and ^{tz}G (blue) at 10 μM in water.

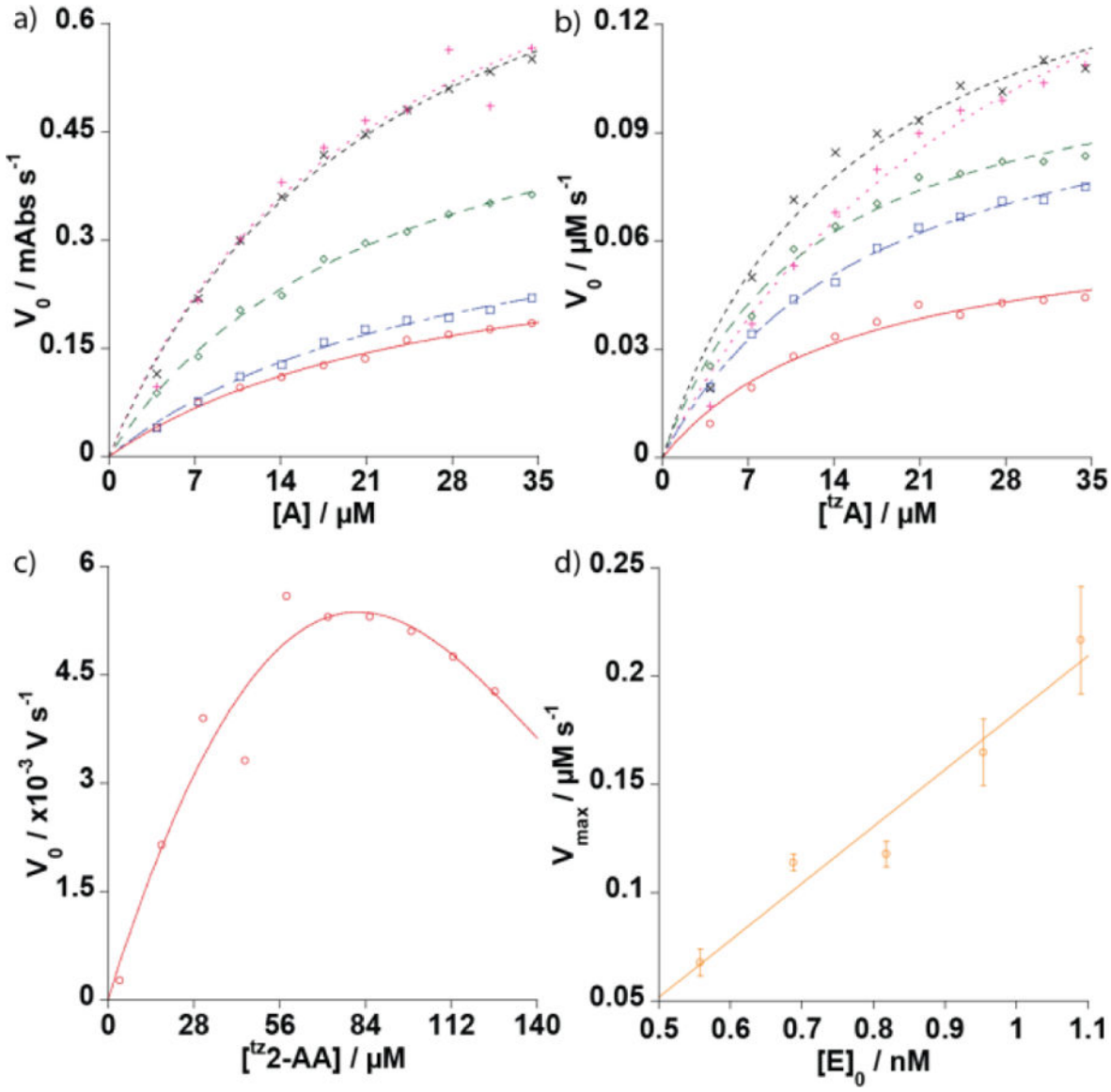

Figure 2.

a, b) Henri-Michaelis-Menten plots of ^{tz}A to ^{tz}I ([^{tz}A] = 3.9–34.5 μM, red, blue, green, black, and pink represent [ADA] = 4.1, 5.1, 6.1, 7.1, and 8.1 mU mL^{-1}) and A to I ([A] = 3.9–34.5 μM, red, blue, green, black, and pink represent [ADA] = 4.1, 5.1, 6.1, 7.1, and 8.1 mU mL^{-1}), c) Competitive inhibition Michaelis-Menten plot with [I] = [^{tz}G] = A*exp(B*[^{tz}2-AA]) of ^{tz}2-AA to ^{tz}G d) V_{max} vs [E]$_0$ plot of ^{tz}A.

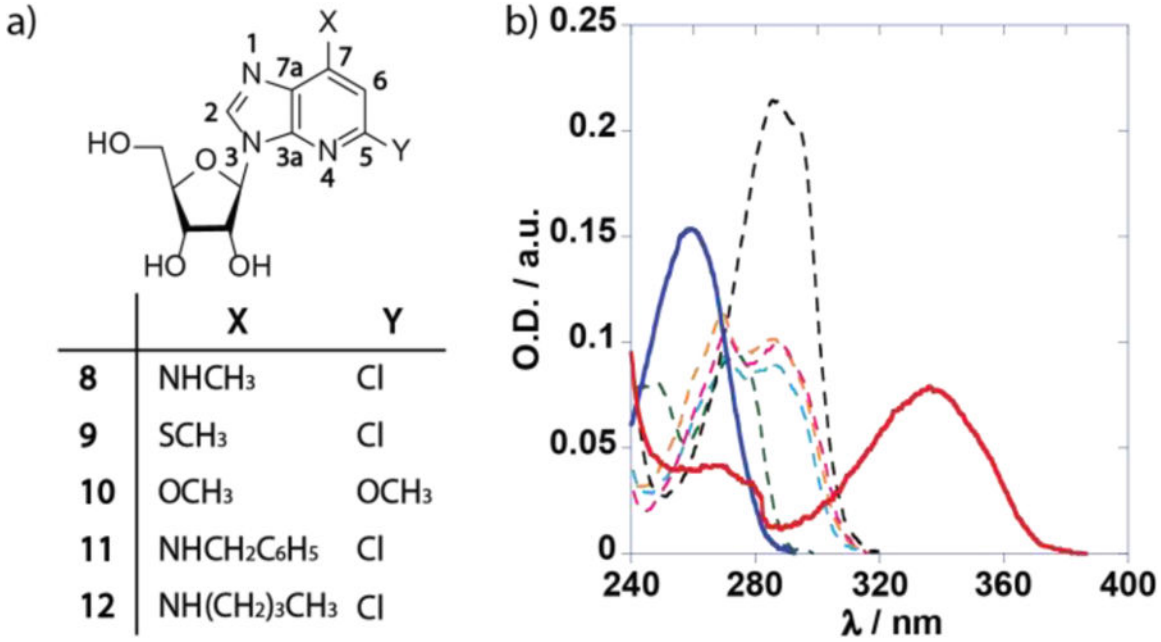

	X	Y
8	$NHCH_3$	Cl
9	SCH_3	Cl
10	OCH_3	OCH_3
11	$NHCH_2C_6H_5$	Cl
12	$NH(CH_2)_3CH_3$	Cl

Figure 3.

a) Structure of potential inhibitors **8**–**12**; b) Absorption spectra of adenosine (solid, blue), ^{tz}A (solid, red), **8** (dashed, orange), **9** (dashed, black), **10** (dashed, green), **11** (dashed, teal), **12** (dashed, pink).

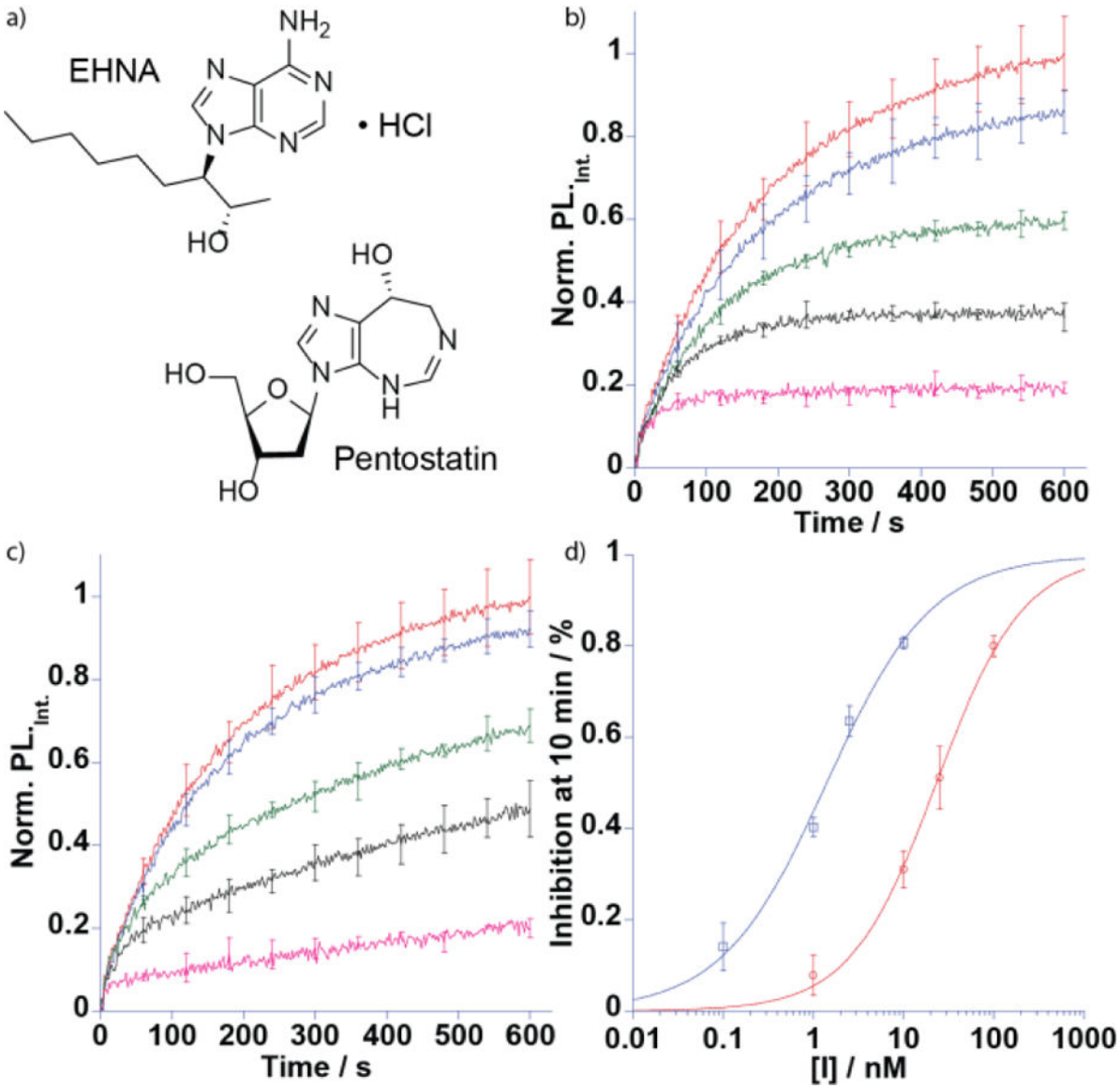

Figure 4.

a) Structures of Pentostatin and EHNA; b, c) conversion of ^{tz}A to ^{tz}I with varying concentrations of Pentostatin (b; red, blue, green, black, and pink lines represent [I] = 0, 0.1, 1, 2.5, 10 nM) and EHNA (c; red, blue, green, black, and pink lines represent [I] = 0, 1, 10, 25, 100 nM); d) Semi-log plot of % inhibition in decimal form after 10 minutes vs. [I] and sigmoidal Hill plot fits for Pentostatin (□, blue line, R^2: 0.990) and EHNA (o, red line, R^2: 0.997).

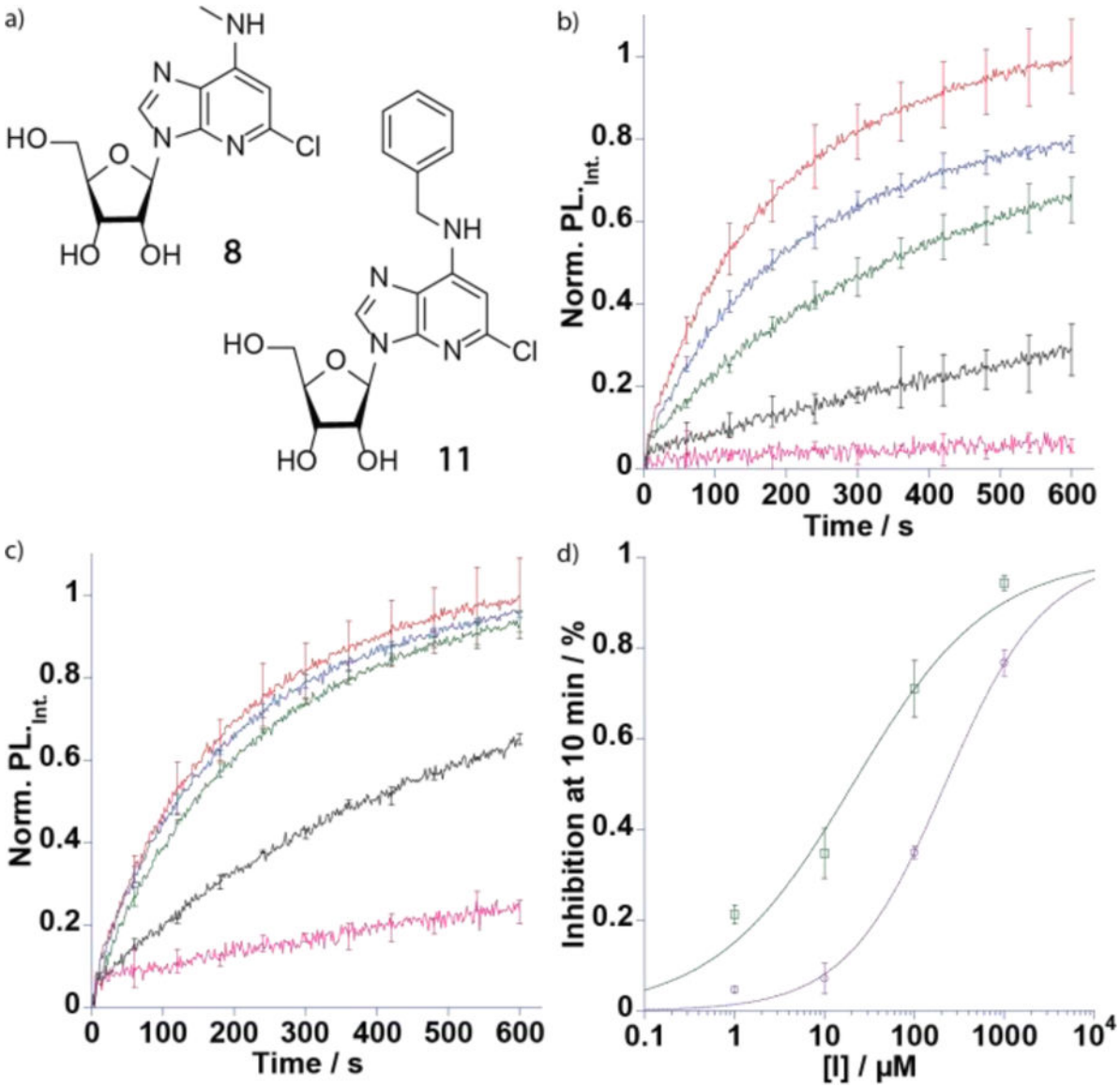

Figure 5.

a) Structures of **8** and **11**; b, c) conversion of ^{tz}A to ^{tz}I with varying concentrations of **8** (b; red, blue, green, black, and pink lines represent [I] = 0, 1, 10, 100, 1000 µM) and **11** (c; red, blue, green, black, and pink lines represent [I] = 0, 1, 10, 100, 1000 µM); d) Semi-log plot of % inhibition in decimal form after 10 minutes vs. [I] and sigmoidal Hill plot fits for **8** (□, green line, R^2: 0.976) and **11** (o, purple line, R^2: 0.997).

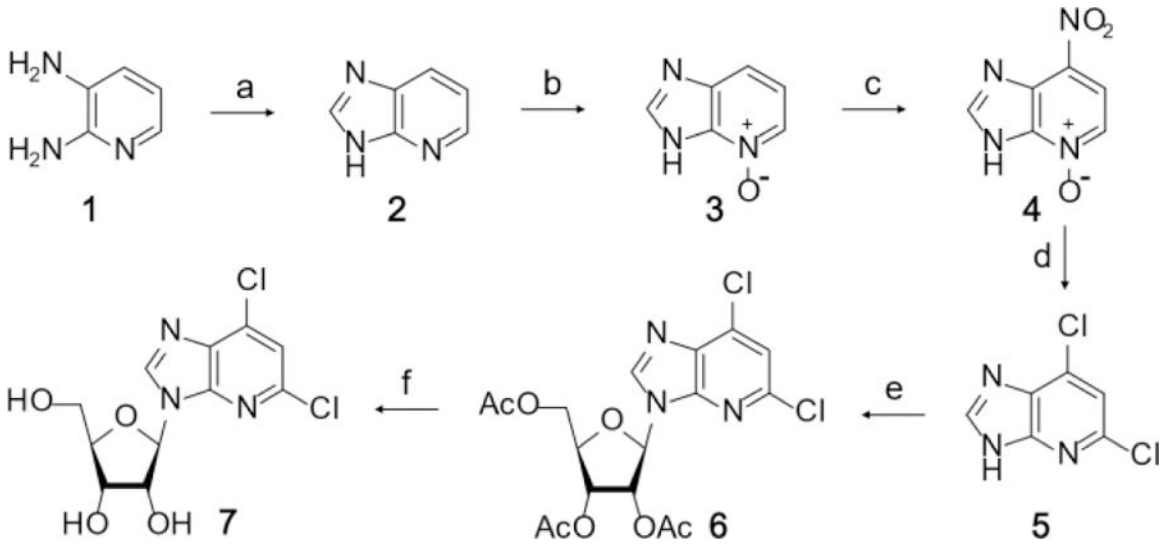

Scheme 1.

Synthetic pathway to key intermediate used to synthesize potential inhibitors. Reagents and Conditions: (a) i. 1, triethylorthoformate, 145^{o}C, 3 h; ii. Formic acid, 110^{o}C, 2 h; iii. MeOH, activated charcoal, rt, overnight, 99%. (b) 2, meta-chloroperbenzoic acid, rt, 72 h, 60%. (c) 3, TFA, 70% nitric acid, 90^{o}C, 4 h, 63%. (d) 4, DMF, phosphoryl chloride, 115^{o}C, 10 m, 50%. (e) 5, TAR, ACN, Tin (IV) chloride, rt, overnight, 82%. (f) 6, MeOH, NH_3, rt, 2 h, 50%.

Table 1.

Experimentally Determined Henri-Michaelis-Menten Parameters.

Compound	$[E]_0$ (mU mL^{-1})	K_M (μM)	V_{max}[a]	R^2
^{tz}A	4.1	15.9±3.4	0.0677±0.0062	0.960
^{tz}A	5.1	17.4±1.3	0.114±0.004	0.995
^{tz}A	6.1	12.4 ± 1.6	0.118±0.006	0.980
^{tz}A	7.1	15.8 ± 3.4	0.165±0.015	0.959
^{tz}A	8.1	32.3 ± 6.4	0.217±0.025	0.982
Adenosine	4.1	27.8 ± 2.9	0.334±0.019	0.993
Adenosine	5.1	29.5 ± 3.8	0.407±0.029	0.991
Adenosine	6.1	22.8 ± 1.8	0.610±0.025	0.995
Adenosine	7.1	22.8 ± 1.8	0.930±0.036	0.996
Adenosine	8.1	22.4 ± 5.5	0.936±0.12	0.960

K_M and V_{max} were calculated using nonlinear regression of ten separate points each performed in triplicate. [a] Adenosine units: mAbs s^{-1};^{tz}A units: Voltage s^{-1}.